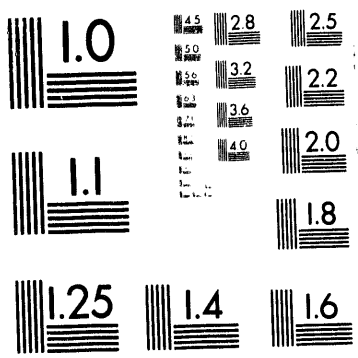
1.0
1.1
1.25
1.4
1.6
2.8
3.2
3.6
4.0
2.5
2.2
2.0
1.8

1 of 1

ORNL/TM-12642

Computing Applications Division

CRITICALITY SAFETY STUDY OF THE MSRE FUEL DRAIN TANK CELL IN BUILDING 7503

D. F. Hollenbach and C. M. Hopper

Date Published: January 1994

Prepared by the
OAK RIDGE NATIONAL LABORATORY
Oak Ridge, Tennessee 37831
managed by
MARTIN MARIETTA ENERGY SYSTEMS, INC.
for the
U.S. DEPARTMENT OF ENERGY
under contract DE-AC05-84OR21400

CONTENTS

LIST OF FIGURES

LIST OF TABLES

ACKNOWLEDGMENTS

We would like to express our gratitude to Mark Ford from the Waste Management and Remedial Action Division for his technical assistance and support. Our thanks also go to Luther Pugh from the Research Reactors Division for sharing his knowledge of the MSRE facility with us, and to Dick Engel, retired, for providing us with first-hand knowledge of the MSRE operations and materials.

ABSTRACT

This report provides a criticality safety study of the molten salt reactor fuel currently being stored in the Fuel Drain Tank (FDT) Cell of the Molten Salt Reactor Experiment (MSRE) facility (Building 7503) located in the Melton Valley area of the Oak Ridge National Laboratory. The FDTs contain approximately 36 kg of uranium consisting primarily of ^{233}U, some plutonium, and fission products in a solidified fluoride salt mixture. The nominal composition of the fluoride salt mixture in the FDTs is 42.16 wt % LiF, 35.79 wt % BeF_2, 21.01 wt % ZrF_4, 1.02 wt % UF_4, and 0.02 wt % PuF_3. The historic criticality safety study does not meet current standards. This work is in support of a new nuclear criticality safety analysis and approval update. Questions concerning the degree of subcriticality associated with the material in its current state and in its most reactive credible upset condition are addressed.

The safety study consists of two parts. In the first part, the FDT Cell was modeled using KENO V.a and analyzed using a variety of cross-section sets. The base FDT Cell model was then modified to represent the most reactive credible upset conditions and analyzed. The second part consists of establishing a benchmark for the FDT Cell. Because of the lack of any other relevant benchmark experiments, the original MSRE was also modeled in KENO V.a and analyzed. The results of the reactor model were then compared with documented MSRE reactor conditions.

The analysis shows that even under the most reactive credible upset conditions, the MSRE FDT Cell is significantly subcritical.

1. INTRODUCTION

The Molten Salt Reactor Experiment (MSRE) was operated from June 1965 to December 1969 to investigate the practicality of using a graphite moderator lattice with molten salt containing uranium as the fuel circulating through channels in the graphite.[1,2] When the reactor was finally shut down, after accumulating 105,737 MWh, the molten salt was transferred into two Fuel Drain Tanks (FDT). The reactor was then flushed with clean salt, which was subsequently stored in one Fuel Flush Tank (FFT). The two FDTs and the FFT are located in the FDT Cell in the MSRE facility. The salt in the FDTs and FFT contains approximately 30.5 kg of ^{233}U, ~6 kg of other uranium isotopes, some plutonium, and accumulated fission products. When the reactor was finally shut down, it was assumed that the facility, fuel salt, and flush salt would probably be utilized at some later date. Therefore, the entire facility was mothballed, and a surveillance and maintenance program was put in place.[3,4]

It eventually became evident that the facility and salt would never be utilized. A decommissioning report was prepared to determine the final disposition of the salt and facility. The decommissioning report recommended removal of the salt and either dismantling or entombment of the hot cells. Because of cost considerations and the lack of any acceptable repository for the salt, alternatives to the decommissioning report recommendations were investigated.

A second report was prepared which examined the problems associated with extended storage of the molten salt *in situ*. It examined the operation limits associated with maintaining the current storage conditions for various time frames. The primary long-term storage limitation is the production of fluorine and free metal from the radiolysis of fluoride salt.[3,4]

Any extended storage of the fluoride salt must take into consideration the criticality safety of the system under normal and credible upset conditions. This report analyzes the FDT Cell in two ways: (1) as it currently exists, and (2) under credible upset conditions. The molten salt reactor, with the original ^{233}U critical loading, is also analyzed as a benchmark. KENO V.a input listings of the nominal configurations for both the FDT Cell and MSRE reactor are contained on the enclosed floppy disk. The objective of this report is to determine if an acceptable level of subcriticality can be maintained and to document the margins of subcriticality utilizing state-of-the-art computational tools. This study provides a technical basis for the subcriticalty evaluation of the MSRE FDT Cell.

2. PROBLEM STATEMENT

The purpose of this work is to determine the margin of subcriticality associated with the MSRE FDT Cell under normal and credible upset conditions. Because it appears that the MSRE fuel will remain in its current state for the near future, an up-to-date criticality assessment of its current state and any credible abnormal state is in order.

2.1 NORMAL CONDITIONS

Currently, the MSRE fuel, in the form of solidified fluoride salt mixture, is stored in two FDTs in the FDT Cell. Small amounts of uranium, plutonium, and fission products are also present in the flush salt. The flush salt, which was used to flush the reactor primary loop after the fuel salt was removed, is stored in the FFT, also located in the FDT Cell.

The FDT is 50 in. in diameter and 86 in. high, with dished top and bottom heads. Each FDT has a total capacity of 80.2 ft^3, which is sufficient to hold all the salt used to fill the reactor primary loop in a subcritical geometry. Inside each FDT is a set of 32 thimbles used by the FDT cooling system. Above each FDT is a cooling system consisting of a steam dome and 32 bayonet tubes inserted in thimbles, which were used to cool the system. An additional thimble, containing a thermocouple, level probes, and salt lines was also not included in the model. Surrounding each tank are banks of heaters and insulation. Figure 1 is a drawing of an FDT.

The FFT is similar to the FDTs. It is 50 in. in diameter, but only 84 in. high, with the same dished top and bottom heads as the FDT. The FDT also lacks the cooling system and bayonet tubes present in the FDTs. The FFT has a storage capacity of 82.2 ft^3 due to the absence of the cooling thimbles. All other material and design considerations are the same as for the FDTs.

The FDT Cell is a sealed rectangular, stainless-steel-lined tank surrounded by reinforced concrete. The cell contains a ventilation system, used to maintain a slight negative pressure, and a small sump containing a jet pump located in the floor. Both the ventilation system and the jet pump have been disconnected and deactivated. Figures 2 and 3 are drawings of the MSRE facility located in Building 7503.

A program of regular surveillance and maintenance has been established since the MSRE was shut down in December 1969. Daily walk-throughs review 27 recorded parameters that include items such as internal cell temperature, personnel radiation monitoring, and cell pressure. A walk-through inspection of all accessible areas of the facility occurs on a monthly basis.

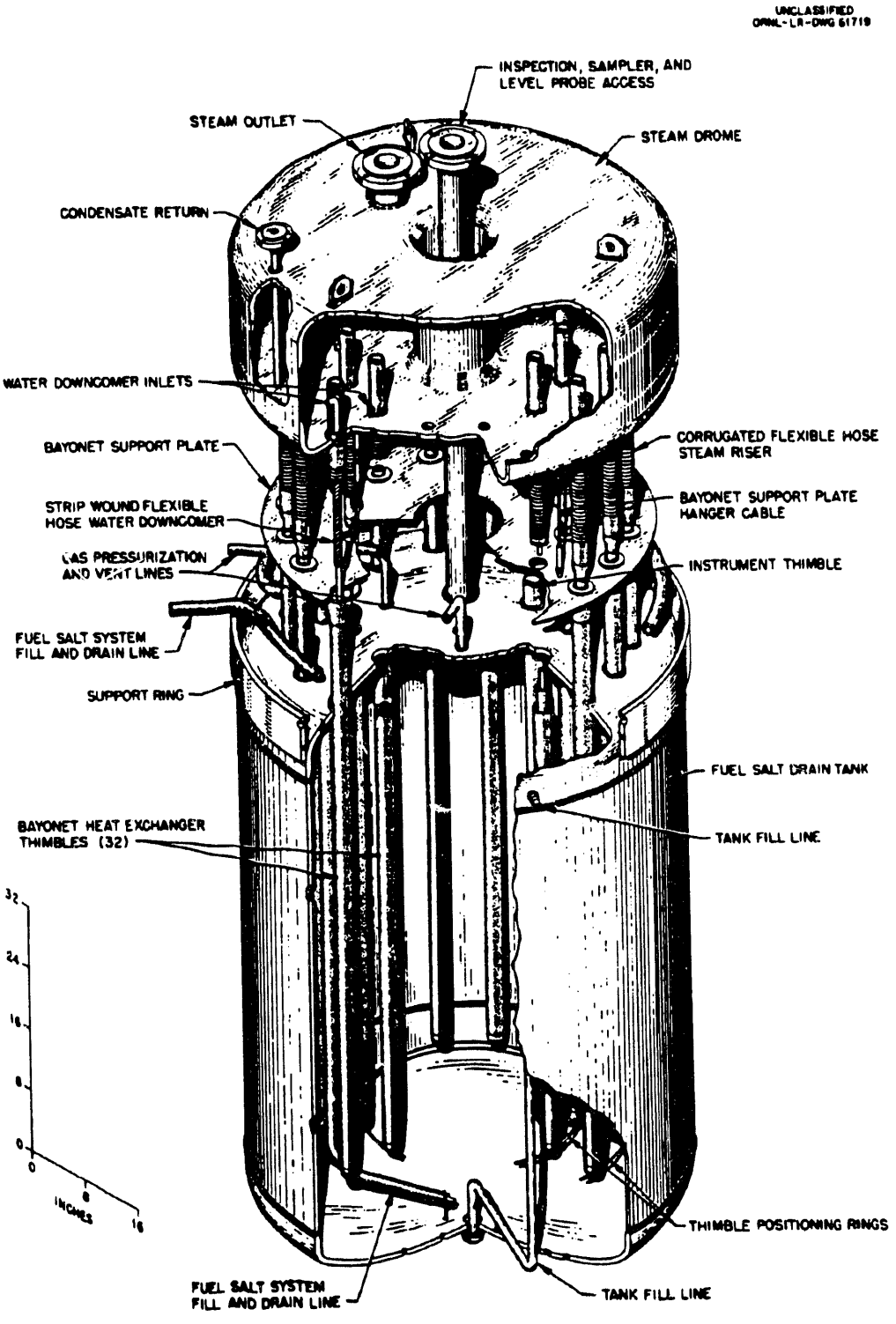

Fig. 1. MSRE fuel-salt drain tank.

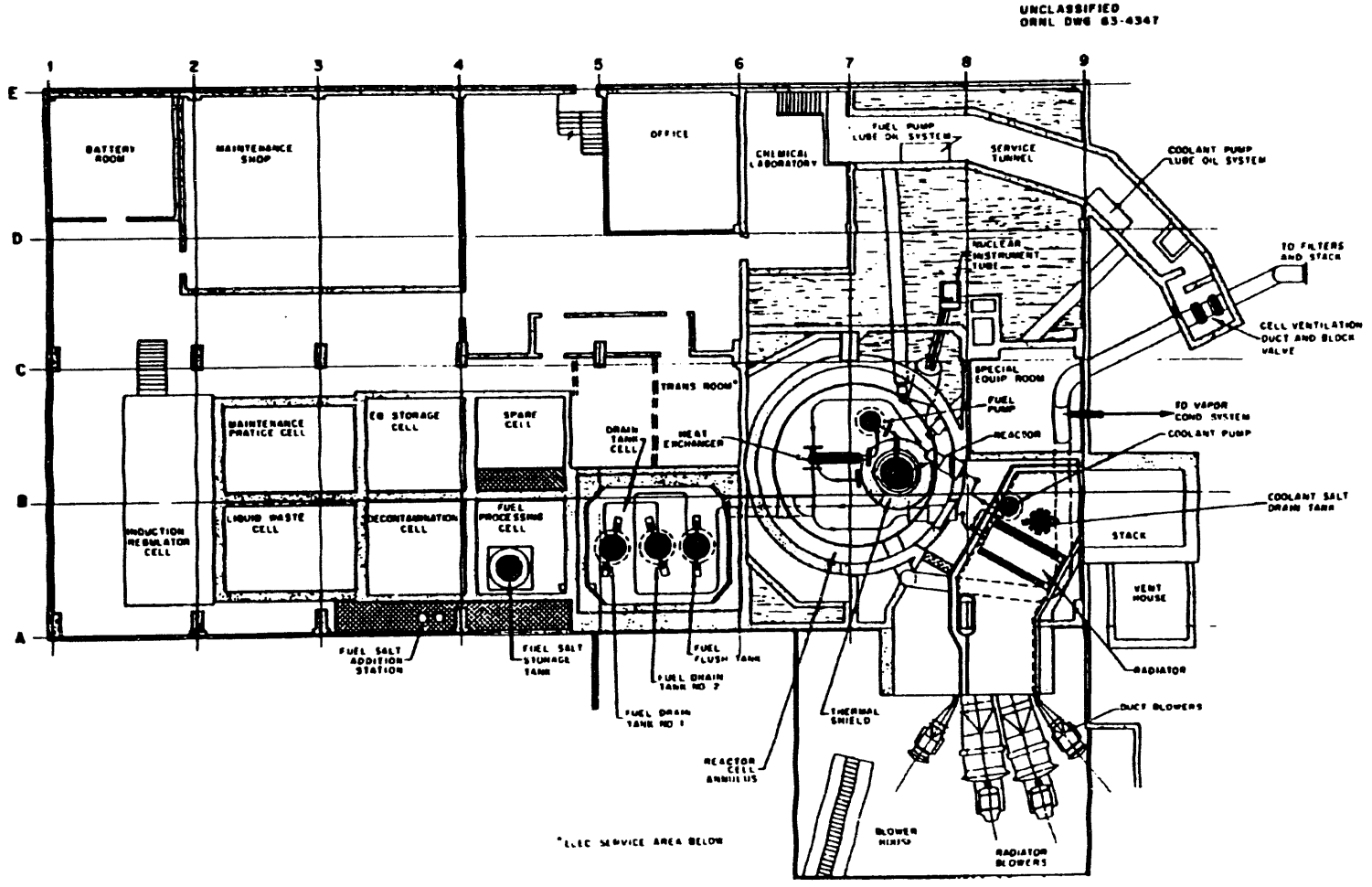

Fig. 2. Basement floor plan of MSRE Facility (Building 7503).

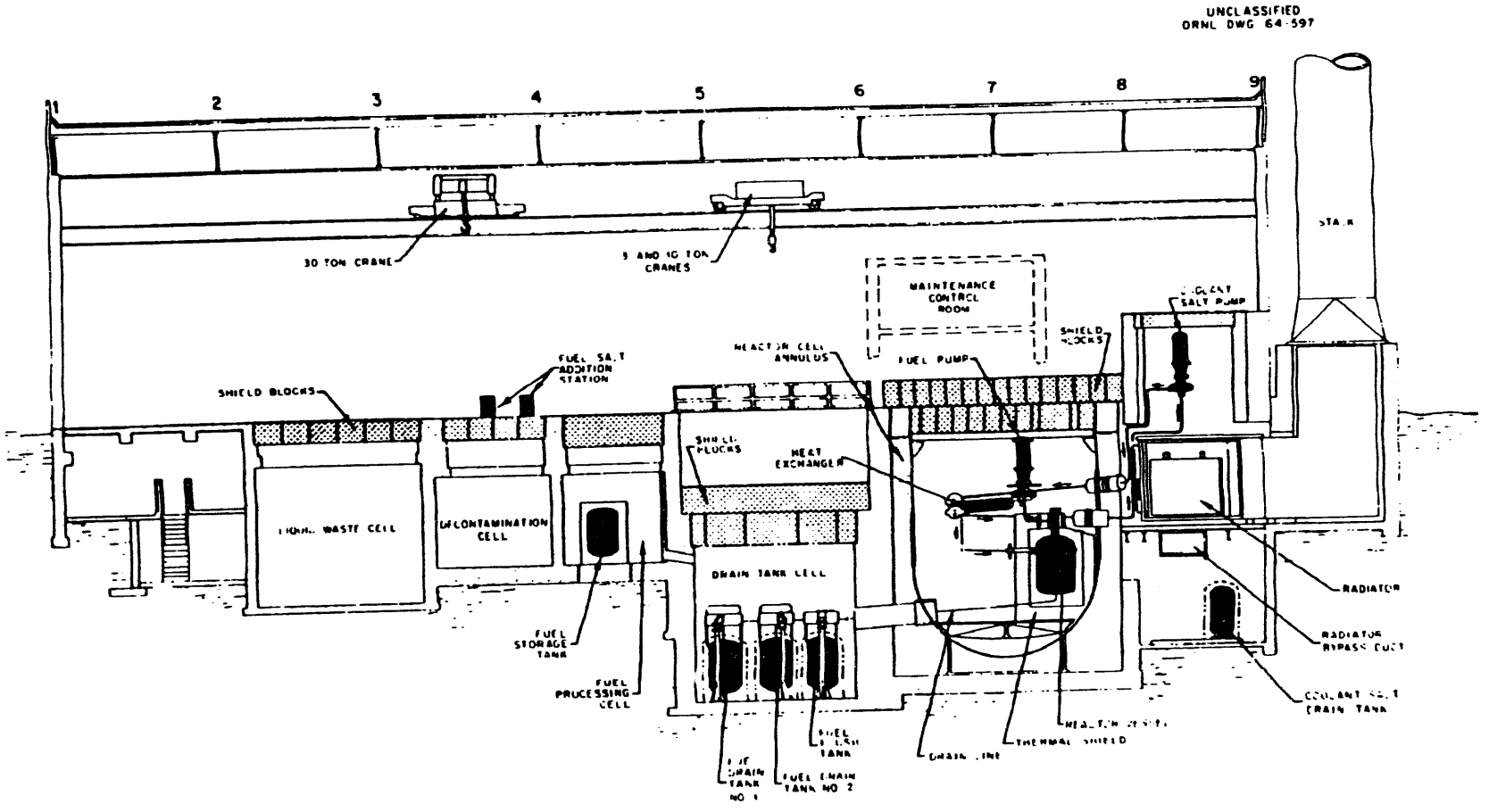

Fig. 3. Elevation view of MSRE Facility (Building 7503).

2.2 ABNORMAL CONDITIONS

The only abnormal condition examined is the movement of the FDTs and FFT from their current position to the most reactive credible geometry. The assumptions used to derive the worst case are as follows. The tanks are assumed to maintain their integrity, with no movement or leakage of fuel salt from either the FDTs or the FFT. The fuel salt is assumed to remain solid, which is reasonable given a melting temperature in excess of 800°F. The thermal shielding initially surrounding the tanks is assumed to have sheared off or crushed, thus allowing the tanks to come in contact. Finally, it is assumed that no water is present in the FDTs, the FFT, or the FDT Cell.

3. MODELING/ANALYSIS

The modeling and analysis of the MSRE is divided into four phases: (1) FDT modeling and analysis using KENO V.a, (2) XSDRN analysis of cross-section libraries, (3) molten salt reactor modeling and analysis using KENO V.a, and (4) comparison of workstation results and Nuclear Criticality Safety System (NCSS) results from the Y12N unclassified IBM mainframe for one FDT and one reactor case using the 27GROUPNDF4 cross-section library. All calculations, except the three using the NCSS software on the IBM mainframe, were performed on ca02, which is an IBM RISC-6000 Model 580 workstation, using SCALE 4.2. The NCSS software on the IBM mainframe uses SCALE 4.0. All KENO V.a runs used the SCALE CSAS25 sequence which processes the cross sections through BONAMI and NITAWL before they are used in KENO V.a.[5] The XSDRN calculations processed the cross sections through BONAMI and NITAWL by running CSASN prior to XSDRN.

This study uses AMPX master format libraries. The libraries provided in the SCALE code system are identified as HANSEN-ROACH and 27GROUPNDF4.[5] The 44GROUPNDF5 and 238GRUPNDF5 libraries were generated, using AMPX, from the ENDF/B-V library and will be available for use in the SCALE code system in the near future.

3.1 FUEL DRAIN TANK MODELING AND ANALYSIS

The primary objective of this work is to determine the degree of subcriticality of the MSRE FDT Cell. To accomplish this, a model of the FDT Cell was created using KENO V.a. This model includes the fuel salt, the flush salt, two FDTs, one FFT, the insulation and canning surrounding the three tanks, the bayonet tubes in the two FDTs, the steam dome above the FDTs (modeled as low-density Hastelloy-N), the support structure for each tank (modeled as low-density SS316), and a SS304 shell for the inside walls of the FDT Cell surrounded by 3 ft of Magnuson concrete. The cell wall shell is, in reality, SS347, and the walls are composed of ordinary concrete to a height of 8 ft above the floor. SS304 was chosen because it was readily available in the cross-section library, and Magnuson concrete was chosen because it produces the largest return neutron-scattering kernel for concrete.[6] The model does not include the heater assemblies surrounding each tank or any other structural material or machinery in the cell. Specifications for the component dimensions and materials came from a set of drawings and reports concerning the drain tanks. The CSAS25 input file for the nominal FDT Cell problem using the 27GROUPNDF4 cross-section library is contained on the floppy disk included in this report.

A certain amount of uncertainty exists concerning the exact composition of the fuel salt in the drain tanks and flush tank. The total salt inventory makeup was initially taken from the

nominal mol percentage values listed in Table 2 of ref. 7. These values sum to 100.004%. As a correction, the listed values were divided by their sum to achieve a total of exactly 100 mol %. The total mass value of fuel salt in the system (4704.5 kg) was also obtained from ref. 7. Using these numbers and an assumed salt density of 2.47 g/cm^3, obtained from Table 2 of ref. 4, a total salt volume of 1,905,870 cm^3 was calculated. The mass and atom densities of the LiF, BeF_2, and ZrF_4 were obtained using these data. The lithium in the salt was assumed to 100% ^{7}Li. The uranium and plutonium total mass and isotopic mass values were then obtained from Table 1 of ref. 7. Using these values, the isotopic concentrations and masses of the UF_4 and PuF_3 were calculated. A final total FDT fuel salt mass was then determined by summing the masses of the LiF, BeF_2, ZrF_4, UF_4, and PuF_3. The final FDT fuel salt mass summed to 4708.8 kg. The percentage of salt in each FDT was determined by dividing the amount of fuel salt in each drain tank by the total amount of fuel salt in both drain tanks, as listed in ref. 8 (p. 1). Table 1 of this report contains a list of the fuel salt parameters used for the FDT Cell calculations.

The total flush salt inventory of 4300 kg was obtained from ref. 8. The salt in the flush tank was assumed to be composed of 66 mol % LiF and 34 mol % BeF_2, as listed in Table 2 of ref. 4. Using these values and an assumed density of 2.47 gm/cm^3, the same as the density of the fuel salt, a total flush salt volume of 1,740,891 cm^3 was calculated. The total and isotopic masses of the uranium and plutonium in the FFT were also obtained from Table 2 of ref. 4. The atom densities and total masses of the uranium and plutonium fluorides were calculated using their respective masses and the FFT salt volume. The uranium and plutonium fluoride masses were added to the previously assumed nonfissile material salt inventory. The parameters of the MSRE flush salt stored in the FFT are listed in Table 2 of this report.

The material composition of Hastelloy-N (previously known as INOR-8) used for all components that came in contact with the fuel or flush salt was obtained from ref. 9. Table 3 lists the elements and their atoms densities that constitute Hastelloy-N.

There are two types of insulation surrounding the fuel and flush tanks. On top of the tanks is FIBERFRAX (type 907-JH). An assumed composition is 51.2% Al_2O_3 and 47.2% SiO_2 at a density of 6 lb/ft^3. The insulation on the bottom and surrounding the tanks, specified as CAREYTEMP 1600 expanded silica, was replaced in the analysis with vermiculite, which is also expanded silica. As specified in the *CRC Handbook of Chemistry and Physics*, 56th Ed. (p. B-201), the chemical composition of vermiculite is $Ca_{0.7}(FeAl)_3Si_8O_{20}(OH)_4(H_2O)_8$. From 49CFR, subpart K, Sect. 178.352-3(d), a density of 0.072 g/cc is specified for vermiculite.

3.1.1 Base Fuel Drain Tank Model

The two FDTs and the FFT were modeled using KENO V.a. The appropriate materials and number densities were used in the modeling of each tank. The tanks were then placed in

Table 1. FDT fuel salt parameters

Parameter	Value
Total fuel salt mass, kg	4,708.8
Fuel salt mass in FDT-1, kg	2,509.8
Fuel salt mass in FDT-2, kg	2,199.0
Fuel salt density, g/cm^3	2.47
Fuel salt volume, cm^3	1,905,870
Total uranium mass in FDTs, kg	36.320
^{233}U	30.479
^{234}U	2.716
^{235}U	0.929
^{236}U	0.038
^{238}U	2.158
Total plutonium mass in FDTs, g	674.79
^{239}Pu	608.20
^{240}Pu	64.24
^{241}Pu	2.35
Fuel salt composition, kg	
LiF	1,985.3
BeF_2	1,685.3
ZrF_4	989.3
UF_4	48.1
PuF_3	0.84

Table 2. FFT fuel flush salt parameters

Parameter	Value
Total flush salt mass, kg	4,300.65
Flush salt density, g/cm^3	2.47
Flush salt volume, cm^3	1,740,891
Total uranium mass in FFT, g	490
^{233}U	190
^{234}U	20
^{235}U	90
^{236}U	0
^{238}U	190
Total plutonium mass in FFT, g	15
^{239}Pu	13
^{240}Pu	2
^{241}Pu	0
Flush salt composition, kg	
LiF	2,226.9
BeF_2	2,073.1
UF_4	0.65

Table 3. Hastelloy-N composition

Material	Atom density (atoms/b-cm)
Nickel (Ni)	6.45×10^{-2}
Molybdenum (Mo)	9.11×10^{-3}
Chromium (Cr)	7.13×10^{-3}
Iron (Fe)	4.74×10^{-3}

a global array and surrounded by stainless steel and Magnuson concrete, as shown in Fig. 4, creating an approximate model of the existing FDT Cell.

The FDT Cell problem was analyzed using four different cross-section libraries. The resulting k_{eff} for each cross-section library is listed in Table 4. The resulting k_{eff} values range from a low of 0.7514 to a high of 0.8602, which represents a spread of about 13%. A fifth calculation was performed, using the 27GROUPNDF4 library, after all insulation and insulation canning were removed from around the three tanks. The competing effects of moderation and absorption seem to cancel out any significance the insulation and canning have on the resulting system k_{eff}.

3.1.2 Credible Upset Condition Model

The most credible upset geometric configuration from a criticality safety standpoint occurs when the 2 FDTs and the FFT separate from their support structures and move next to each other in a corner. In this event it is assumed the surrounding canning and insulation are removed from each tank. This positions the fissile material in the tanks as close together as is physically possible with the maximum possible reflection in the FDT Cell given the assumed constraint of no water ingress. The cell walls are assumed to be Magnuson concrete with a SS304 liner. Magnuson concrete provides the largest reflection kernel of all the concretes currently available in the used cross-section libraries as shown in ref. 6. A schematic of this configuration is shown in Fig. 5. The k_{eff} for this problem using the 27GROUPNDF4 cross-section library was 0.9067 with a standard deviation of 0.0018.

3.1.3 Fuel Drain Tank Sensitivity Studies

A significant amount of uncertainty surrounds the total amount of fuel salt in the FDTs and the actual fissionable material content. To help bound this uncertainty, several problems involving small changes in one parameter from the base case were made and then the resulting k_{eff} compared with the base case, which has a $k_{eff} = 0.8602$ (± 0.0021). All these problems used the 27GROUPNDF4 cross-section library. The percentage change from the base case was then calculated. Table 5 contains the altered problems, their k_{eff} values, and the percentage change from the base case.

The first two problems in Table 5 involve a $\pm 5\%$ change in the fissile fuel (uranium and plutonium) content in the FDT salt. These changes in fissile material resulted in less than a 1.5% change in the k_{eff} of the system. The third and fourth problems, listed in Table 5, show the effects of a $\pm 5\%$ change in FDT salt density. The FDT Cell is a very undermoderated system. The addition of fluoride salt to the system reduces the average energy of the neutrons,

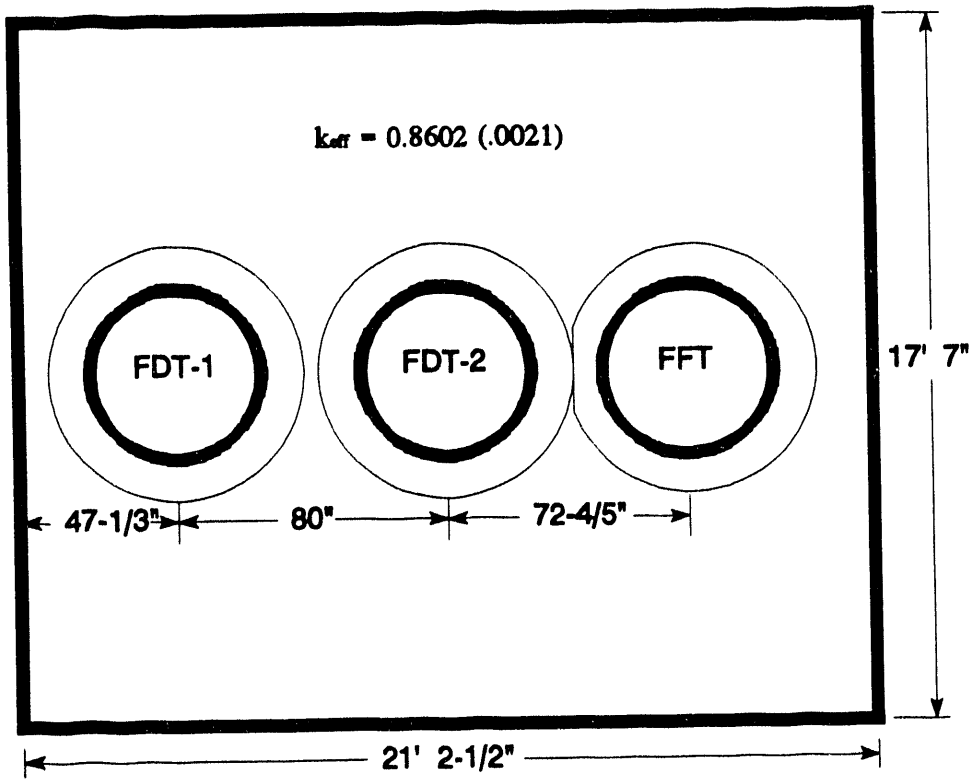

Fig. 4. Schematic of normal FDT Cell configuration.

Table 4. MSRE FDT k_{eff} calculations for various cross-section libraries using KENO V.a

Cross-section library	k_{eff} ($\pm\sigma$)
Hansen-Roach	0.7514 (0.0015)
27GROUPNDF4	0.8602 (0.0021)
44GROUPNDF5	0.8468 (0.0016)
238GROUPNDF5	0.8145 (0.0018)
27GROUPNDF4[a]	0.8579 (0.0018)

[a]Insulation and canning removed from around FDTs and flush tank.

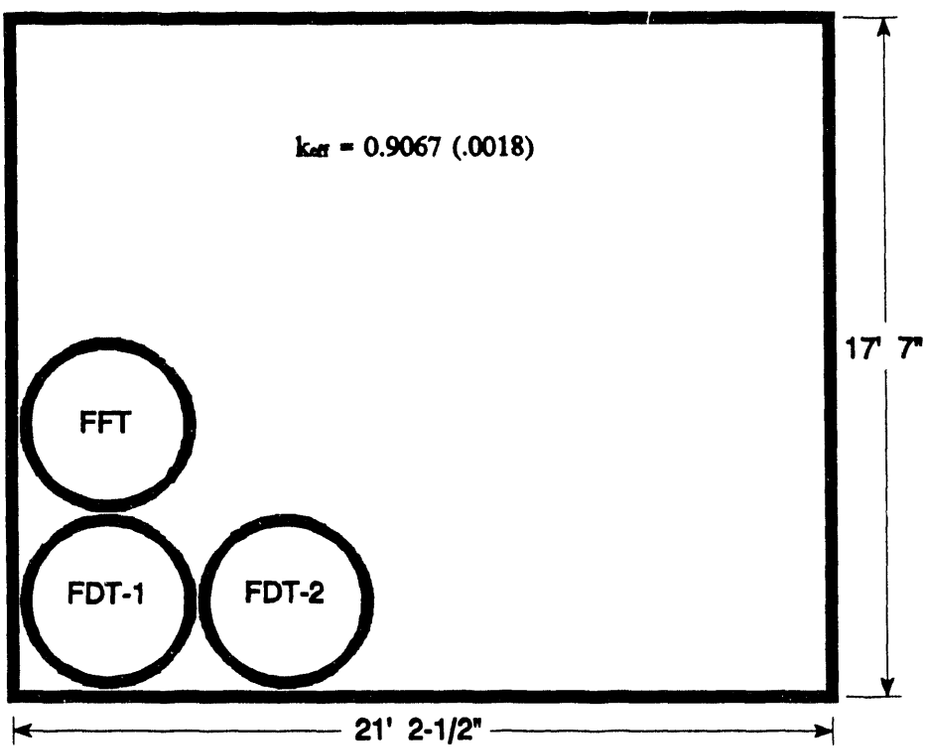

Fig. 5. Schematic of most reactive credible FDT Cell configuration.

Table 5. Sensitivity study of FDT parameters[a]

Problem	k_{eff} ($\pm\sigma$)	% change
5% Decrease in U and Pu density in FDT-1 and -2	0.8474 (0.0020)	-1.49
5% Increase in U and Pu density in FDT-1 and -2	0.8798 (0.0020)	1.28
5% Decrease in salt density in FDT-1 and -2	0.8161 (0.0019)	-5.13
5% Increase in salt density in FDT-1 and -2	0.8966 (0.0019)	4.23
Bayonet tubes removed in FDT-1 and -2	0.8925 (0.0019)	3.75
10% Increase in FDT-1 salt volume at nominal density removed from FDT-2	0.8896 (0.0016)	3.42
Bare FDT-1 (fuel and tank only)	0.8547 (0.0017)	-0.64
FDT-1 (fuel and tank) with tight SS304 and Magnuson concrete reflector	0.8754 (0.0017)	1.77
FDT Cell base case at 260°C	0.8534 (0.0018)	-0.79
FDT Cell most reactive case at 20°C	0.9067 (0.0018)	5.41
FDT Cell most reactive case at 260°C	0.9026 (0.0015)	4.93

[a]Changes measured from a base of k_{eff} = 0.8602($\pm$0.0021)

thus increasing the k_{eff} of the system. A 5% change in salt density correlates to approximately a 5% change in the k_{eff} of the FDT Cell.

The fifth problem listed in Table 5 shows the effect the thimbles and bayonet tubes have on the system. The thimbles and bayonet tubes are made of Hastelloy-N which is an effective neutron absorber. Unlike the bayonet tubes, the thimbles are permanently welded to the FDT head and cannot be removed without breaching the FDT. In this problem, the thimbles and bayonet tubes are replaced with void in FDT-1 and -2. The 3.75% increase in k_{eff} resulting from their removal is indicative of the strong neutron absorption characteristics of the material.

The sixth problem in Table 5 shows the effect of shifting fluoride salt from FDT-2 to FDT-1. The fuel salt in FDT-1 was increased by 10%, with a corresponding decrease in the fuel salt content in FDT-2. This shift in fuel salt results in an increase in the system k_{eff} by 3.42%.

The seventh and eighth problems listed in Table 5 involve FDT-1 alone, with the insulation and canning removed. The first of the two problems is FDT-1 alone surrounded by void. The k_{eff} of FDT-1 alone is only 0.64% lower than that of the FDT Cell. The second of the two problems is the same as the above problem, with a tight-fitting stainless steel liner and concrete reflector. The reflector produces a 1.76% increase in the k_{eff} relative to the base case

and a 2.41% increase over the bare FDT-1 case. These changes indicate that the FDTs are essentially independent of each other, and the one with the most fuel salt and the best reflection will be the one that is responsible for the majority of the reactivity of the system. Approximately one-third to one-half of the 5% gain in reactivity between the base case and the nominal credible accident case is due to the increased reflection of a unit.

The last three problems in Table 5 show the effect of increasing the temperature of the salt and tanks. Increasing the temperature to 260°C for both the base case and worst credible geometric configuration resulted in less than a 1% change in reactivity. This lack of significant change with temperature shows that the FDT Cell reactivity is insensitive to temperature in the allowed range and that reactivity decreases as temperature decreases, as expected.

3.2 XSDRN ANALYSIS OF CROSS-SECTION LIBRARIES

To help better understand what caused the large differences in k_{eff} between cross-section libraries, a simplified one-dimensional (1-D) FDT was modeled as a sphere using XSDRN. The innermost region of the sphere contains the total volume of fuel salt present in both FDTs. The sphere modeled in XSDRN consisted of seven regions. Beginning with the innermost region, the regions consist of fuel salt, Hastelloy-N, SS304, vermiculite, SS304, void, and Magnuson concrete. Cross sections were preprocessed through CSASN, which runs BONAMI and NITAWL, prior to being used in XSDRN. The cross sections were then collapsed to equivalent 16-group cross-section sets for comparison. Significant differences were observed between the different cross sections for several materials. Values for LAMBDA (the XSDRN term for k_{eff}) were calculated using this model with each of the cross-section libraries previously listed. Values of LAMBDA from each cross-section library are shown in Table 6. However, the variation in the LAMBDA values in Table 6 seem to mimic the k_{eff} values in Table 4.

3.3 MOLTEN SALT REACTOR MODELING AND ANALYSIS

A validation benchmark for the FDT problem was needed to give some confidence that the values being calculated had some basis in reality. Since no acceptable benchmark could be found in the literature, the benchmark chosen was the MSRE reactor in its initial critical state after the initial ^{233}U fuel loading. The configuration of the reactor was modeled in KENO V.a .eometry based on a set of related drawings listed in Appendix A. All reactor components were made of Hastelloy-N, except the moderating material, which was composed of graphite at a density of 1.83 g/cm^3 and the control rods. The reactor assembly consists of the reactor surrounded on the sides and top by canned vermiculite insulation and a thermal shield consisting of ball bearings, H_2O, and potassium nitrite (KNO) as a corrosion inhibitor. Because of the

Table 6. MSRE FDT LAMBDA calculations for various cross-section libraries using XSDRN

Cross-section library	LAMBDA
Hansen-Roach	1.11336
27GROUPNDF4	1.17227
44GROUPNDF5	1.15556
238GROUPNDF5	1.13288

enormous amount of material contained in the insulation and thermal shield around and above the reactor, the entire MSRE reactor cell with all the equipment surrounding the reactor assembly was not modeled. Instead, the reactor model consists of the reactor assembly sitting on 2 ft of Magnuson concrete.

The reactor fuel salt composition, excluding the uranium and plutonium, was obtained using ref. 10 (p. 9). The salt was assumed to be composed of LiF-BeF_2-ZrF_4, with mol percents of 64.7, 30.1, and 5.2, respectively. The density of the material was obtained using the following equation from the same reference:

$$\rho(g/cm^3) = 2.5387 - 5.769 \times 10^{-4} * t(°C).$$

The fuel salt and moderator were assumed to be at a temperature of 650°C, which is the reactor operating temperature. After the composition of the above salt was determined, the uranium and plutonium were separately added to the salt mixture, assuming a density of 15.11 g/L as specified in Table 7 (p. 54) of ref. 11. The parameters of the MSRE fuel salt in the reactor are listed in Table 7.

The uranium isotopic composition was calculated based on the 33.380 kg of uranium added to the system having an isotopic composition shown in Table 1 of ref. 11, a 1.935-kg heel of uranium assayed at 32.97% ^{235}U and 66.23% ^{238}U, as specified in ref. 11 (p. 21), and 0.89 kg of depleted uranium (assumed 99.8% ^{238}U and 0.2% ^{235}U) as specified in ref. 11 (p. 21). The uranium was assumed to be present in the form of UF_4.

A density of plutonium was then calculated relative to the amount of uranium present in the system. The total amount of plutonium and its isotopic distribution in the fuel circuit are shown in Table 3.6 (p. 59 of ref. 12). The values used are those shown for fuel circuit inventory, run 20-I. A plutonium density was calculated by dividing the total amount of plutonium by the total amount of uranium and multiplying the result by the uranium density. Given the plutonium density and isotopic composition, densities for the plutonium in the system were calculated.

Table 7. MSRE reactor fuel salt parameters

Parameter	Value
Total fuel salt mass, kg	4,707.5
Total fuel salt density, g/cm^3	2.1637
Uranium density in salt, g/l	15.11
Total uranium mass in FDTs, kg	36.2050
^{232}U	0.0066
^{233}U	30.5265
^{234}U	2.5467
^{235}U	0.8753
^{236}U	0.0324
^{238}U	2.2175
Total plutonium mass in FDTs, g	690
^{239}Pu	625.80
^{240}Pu	61.81
^{241}Pu	2.39
Fuel salt composition, mol %	
LiF	64.7
BeF_2	30.1
ZrF_4	5.2

The control rods were the last significant component to be modeled in the reactor system. The control rod neutron-absorbing material consists of 70 wt % Gd_2O_3 and 30 wt % Al_2O_3. The control rod material is a ceramic sintered to a minimum of 95% theoretical density. The control rod elements consist of the absorbing material formed in a ring and canned in Inconel. The elements were then threaded on a helically wound, flexible stainless steel hose with two braided Inconel cables running through it. Four sealed inconel thimbles ran from the top of the reactor to the bottom of the graphite lattice. Each of the three control rods moved in a separate guide thimble. The fourth thimble contained corrosion specimens. A description of the control-rod elements is given in ref. 13. Figure 6 is a drawing of the Molten Salt Reactor. The CSAS25 input file for the nominal reactor problem using the 27GROUPNDF4 cross-section library is contained on the floppy disk included in this report.

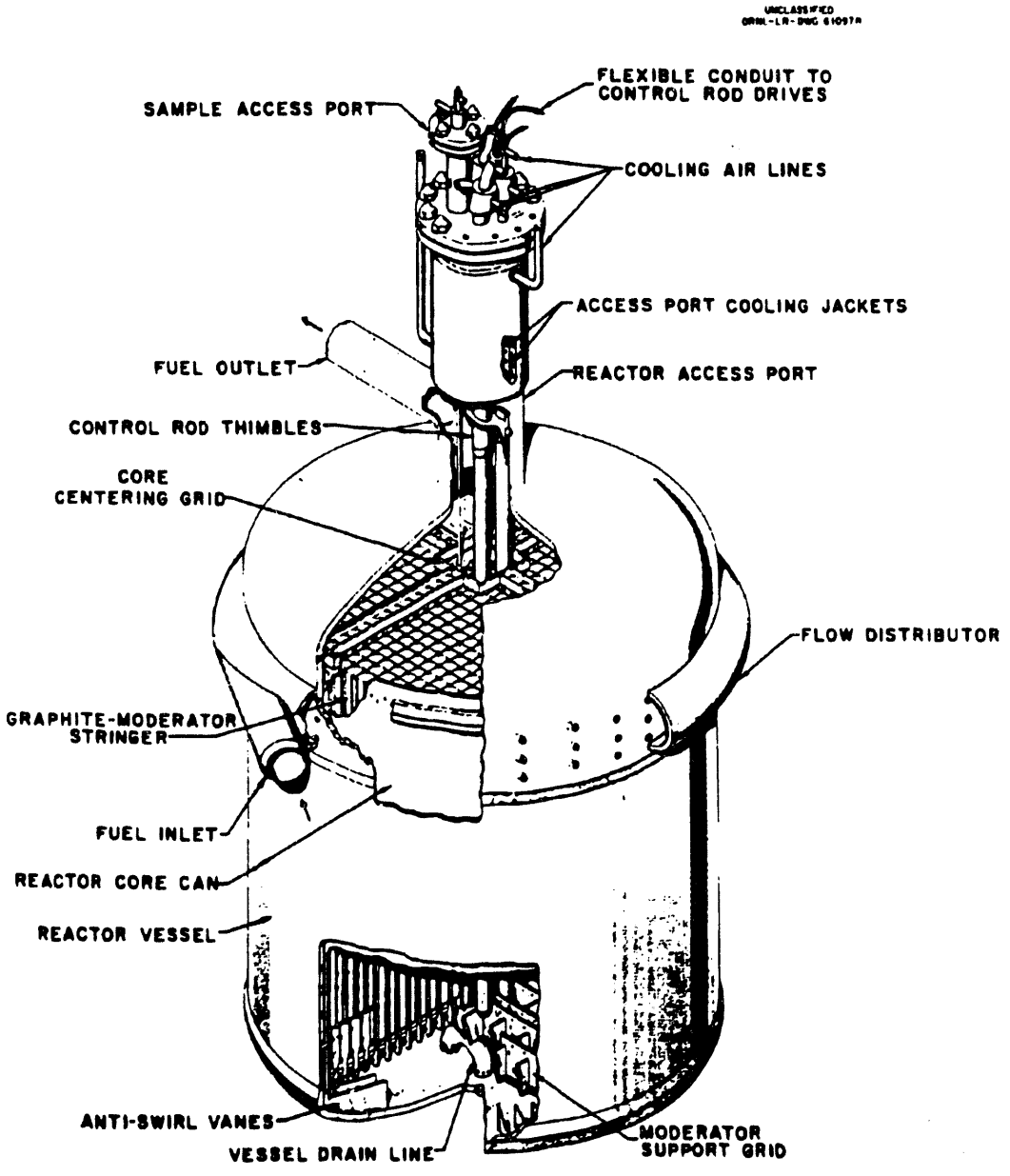

Fig. 6. A schematic of the Molten Salt Reactor.

3.3.1 Base Reactor Model

After a model of the reactor system was completed and the material compositions determined, the k_{eff} of the system was calculated using each of the above-mentioned four cross-section libraries. In all calculations the control rods were assumed to be fully withdrawn at 51 in. as specified in Fig. 2 of ref. 14 (p. 6). The results from these calculations, ranging from a low of 0.9805 to a high of 1.0276, are shown in Table 8. For the reactor model, the values of k_{eff} differ by about 5% as compared with 13% for the drain tank cell model.

The relatively good agreement between cross-section groups is somewhat surprising given the magnitude of the differences seen for the FDT Cell. Although the material specification of the fluoride fuel salt in the FDTs is almost identical to the material specification of the fluoride fuel salt in the reactor, there are two significant differences. The reactor is essentially a thermal system from the standpoint of neutron energy, whereas the FDT Cell is an epithermal system. The FDT Cell is at room temperature whereas the reactor is at 650°C. The cross-section sets were generated for systems with thermal neutron energies and are therefore expected to better represent thermal systems than epithermal systems.

3.3.2 Reactor Sensitivity Studies

Just as there is some uncertainty related to the material content of the two FDTs, there is some amount of uncertainty related to the actual material content in the reactor. To help bound this uncertainty, $\pm 5\%$ changes were made to certain key material densities and compared with the base case, which has a k_{eff} = 1.0049 (± 0.0017). All these problems used the 27GROUPNDF4 cross-section library. The k_{eff} and percentage change from the base case were then calculated for each problem. Table 9 contains the altered problems, their k_{eff} values, and the percentage change from the base case.

The first two problems in Table 9 involve a $\pm 5\%$ change in the material density of the control rod absorber in the reactor. These changes result in changes in the k_{eff} of the system that are within the statistics of the problem. The control rods in these problems are in the fully withdrawn position, with only about 1 [illegible] of absorber material in the moderated section of the reactor. The control rods have little effect in this position, as is shown in the results of the altered problems.

The third and fourth problems listed in Table 9 show the effects of a $\pm 5\%$ change in the fissile fuel density. In these two problems only the uranium and plutonium content were altered. The changes in k_{eff} track the changes in fuel density, with a -2.29% change in k_{eff}, corresponding to a 5% decrease in fissile material density, and a 1.94% increase in k_{eff}, corresponding to a 5% increase in fissile material density.

Table 8. MSRE reactor k_{eff} calculations[a] for various cross-section libraries using KENO V.a

Cross-section library	k_{eff} ($\pm\sigma$)
Hansen-Roach	1.0276 (0.0017)
27GROUPNDF4	1.0049 (0.0017)
44GROUPNDF5	0.9805 (0.0016)
238GROUPNDF5	0.9873 (0.0016)

[a]Rod position at 51 in.

Table 9. Reactor sensitivity studies

Problem	k_{eff} ($\pm\sigma$)	% change[a]
5% Decrease in the control rod material density	1.0053 (0.0016)	0.04
5% Increase in the control rod material density	1.0015 (0.0015)	-0.34
5% Decrease in U and Pu density	0.9819 (0.0015)	-2.29
5% Increase in U and Pu density	1.0244 (0.0017)	1.94
5% Decrease in graphite density	0.9833 (0.0015)	-2.15
5% Increase in graphite density	1.0191 (0.0013)	1.41
5% Decrease in salt density	0.9981 (0.0015)	-0.68
5% Increase in salt density	1.0101 (0.0015)	0.52
Temperature decreased to 20°C	1.0666 (0.0015)	6.14

[a] % changes measured from a base case k_{eff} = 1.0049 ($\pm$0.0017).

The fifth and sixth problems in Table 9 involve a ±5% change in the graphite moderator density. The graphite moderator in the reactor is composed of long (~50-in.) rectangular stringers in a lattice, with notches cut out of each side. Fuel salt flows through the notches cut in the stringers. The change in moderator density has the same level of effect as the change in fissile material density. This situation exists because the system is undermoderated, so any additional moderation increases the reactivity of the system.

The seventh and eighth problems in Table 9 represent the effects of a ±5% change in the fluoride salt density while maintaining the base fissile fuel density. The addition of fluoride salt to the system reduces the average energy level of the neutrons, thus increasing the k_{eff} of the system. The changes in salt density mimic the changes in moderator density for the same reasons but to a smaller degree. A 5% change in salt density correlates to less than a 1% change in the k_{eff} of the reactor system.

The last problem shows the reactivity effect of reducing the salt temperature to 20°C. Bringing the salt to room temperatures adds over 6% reactivity to the system. Although this is a lot of excess reactivity, the control rods have sufficient negative reactivity so that when totally inserted the reactor should be subcritical.

3.3.3 Control Rod Insertion Model

Considering the range of k_{eff} values for different cross-section sets, another measure of the accuracy of the reactor model was considered useful. Instead of just the k_{eff} of the system, the change in reactivity of the system with respect to rod height was compared for the 238GROUPNDF5 and the 27GROUPNDF4 cross sections. The excess reactivity of the system ($\delta k_{eff}/k_{eff}$) was calculated for each rod position. The excess reactivity calculation used the fully withdrawn position (51 in.) as the base k_{eff}.

The positions of the three control rods were altered from 51 in. (fully withdrawn) to 0 in. (fully inserted). The k_{eff} values of the system with the control rods in five different positions were calculated using the 27GROUPNDF4 and the 238GROUPNDF5 cross sections. The three control rods were moved as a bank. The results of the calculation are shown in Tables 10 and 11.

The percentage change in reactivity seems to agree reasonably well between cross-section groups, although the 238GROUPNDF5 results are approximately 1% higher for each case. A portion of the differences can be attributed to the gadolinium used in the two cross-section libraries. For the two cross-section sets, the gadolinium control rod material is specified differently. In the 27GROUPNDF4 cross-section library, gadolinium is specified as a material with natural isotope concentrations. In the 238GROUPNDF5 cross-section library gadolinium is specified as a set of isotopes that must be mixed proportionally to produce natural gadolinium.

Table 10. MSRE reactor k_{eff} calculations for various control rod positions using the 27GROUPNDF4 cross-section library for all three control rods moved as a bank

Control rod position (in.)	k_{eff} ($\pm\sigma$)	$\%\delta k_{eff}/k_{eff}$[a]
0.0	0.9393 (0.0017)	6.53
14.0	0.9577 (0.0016)	4.70
29.0	0.9837 (0.0016)	2.11
36.0	0.9909 (0.0016)	1.39
51.0	1.0049 (0.0017)	0.0

[a] $\delta k_{eff}/k_{eff}$ = (k_{eff} (51.0 in.) minus k_{eff} (rod position)) / k_{eff} (51.0 in.).

Table 11. MSRE reactor k_{eff} calculations for various control rod positions using the 238GROUPNDF5 cross-section library for all three control rods moved as a bank

Control rod position (in.)	k_{eff} ($\pm\sigma$)	$\%\delta k_{eff}/k_{eff}$[a]
0.0	0.9132 (0.0015)	7.50
14.0	0.9333 (0.0015)	5.47
29.0	0.9568 (0.0016)	3.09
36.0	0.9644 (0.0016)	2.32
51.0	0.9873 (0.0016)	0.00

[a] $\delta k_{eff}/k_{eff}$ = (k_{eff} (51.0 in.) minus k_{eff} (rod position)) / k_{eff} (51.0 in.).

The gadolinium was assumed to have a natural isotopic ratio at a specified density. In addition, the 27GROUPNDF4 library's ^{233}U cross sections assumed infinite dilution, so no self-shielding is present, and there is no temperature dependence.

Another method of benchmarking the reactor is to compare the percentage excess reactivity as a function of rod height with the curve of reactivity poisoning per rod position given in ref. 11. The results of the calculations using the 27GROUPNDF4 cross-section library and the k_{eff} of the fully withdrawn position (51 in.) as the base case are given in Table 12. Figure 7 is the reactivity curve from ref. 11, with the results from Table 12 plotted on top.

Table 12. MSRE reactor k_{eff} calculations for various control rod No. 1 positions with control rods 2 and 3 at 51 in. using the 27GROUPNDF4 cross-section library

Control rod position (in.)	k_{eff} ($\pm\sigma$)	$\%\delta k_{eff}/k_{eff}$[a]
0	0.9743 (0.0017)	3.00
8	0.9806 (0.0017)	2.41
16	0.9851 (0.0018)	1.97
24	0.9905 (0.0019)	1.43
32	0.9986 (0.0015)	0.63
40	1.0010 (0.0016)	0.39
48	1.0037 (0.0015)	0.12
51	1.0049 (0.0017)	0.00

[a] $\delta k_{eff}/k_{eff}$ = (k_{eff} (51.0 in.) minus k_{eff} (rod position)) / k_{eff} (51.0 in.).

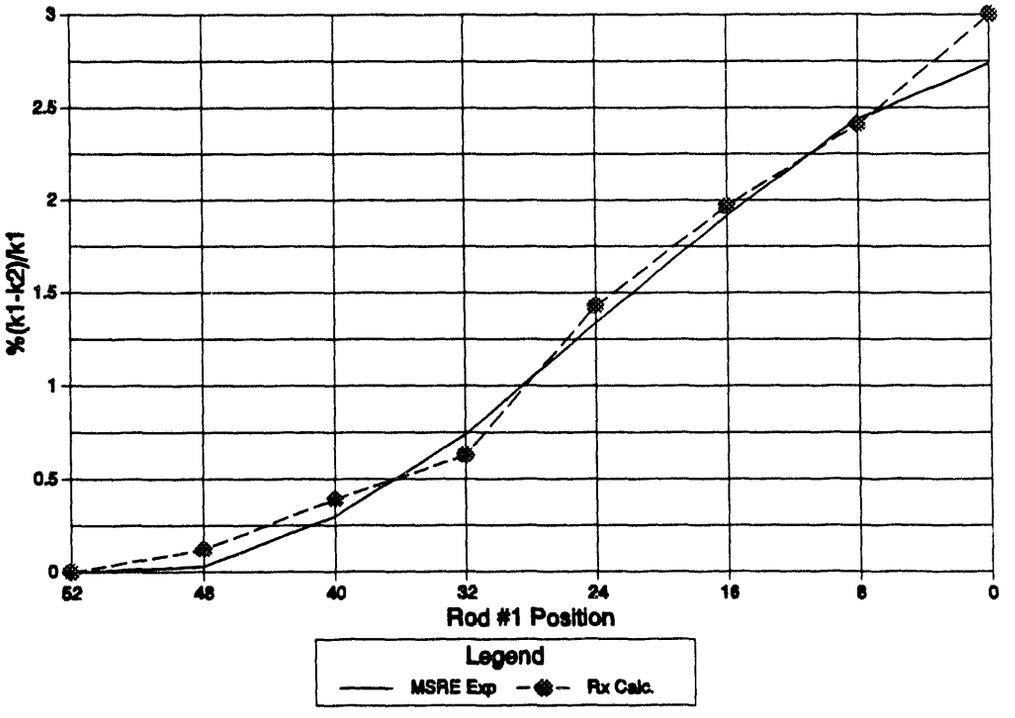

Fig. 7. Comparison of percentage change in reactivity of the original MSRE and the KENO V.a model calculations with respect to rod No. 1 position.

The solid line in Fig. 7 represents the percentage change in reactivity originally measured in the MSRE reactor at various control rod positions. The dashed line with circles represents the percentage change in reactivity calculated by the KENO V.a model. As shown in Fig. 7, the percentage change in reactivity calculated using the KENO V.a model of the reactor is in good agreement with the experimental results.

3.4 COMPARISON OF WORKSTATION AND NCSS RESULTS

All the previous calculations were done on CA02, which is an IBM RISC-6000 Model 580 workstation, using a controlled version of SCALE 4.2. Although controlled, the SCALE system used does not meet all QA requirements. To show that the results are acceptable, two FDT cases and one reactor case were run on the Y12N IBM mainframe using the QA, NCSS version of SCALE. All three cases used the CSAS25 program having the creation data of 92.014, utilizing the library NCSS.ZAZ39461.VIR000.S000.LOAD. The results of these and the corresponding workstation cases are listed in Table 13. The NCSS and workstation results agree within 2σ for the three problems. This agreement indicates that the workstation results can be considered reliable.

Table 13. Comparison of workstation results to NCSS results from Y12N for one reactor and one drain tank problem[a]

System	Workstation k_{eff} ($\pm\sigma$)	NX10a NCSS k_{eff} ($\pm\sigma$)
Fuel drain tank (Normal configuration)	0.8602 (0.0021)	0.8572 (.0018)
Fuel drain tank (Most reactive geometry)	0.9067 (0.0018)	0.9052 (.0016)
Reactor[b]	1.0049 (0.0017)	1.0067 (.0017)

[a]27GROUPNDF4 cross-section library.
[b]Rods at 51-in. position.

4. DISCUSSION AND CONCLUSIONS

The objective of this report is to show that the FDT Cell will maintain an acceptable level of subcriticality under all normal and credible abnormal upset conditions. Accomplishing this goal required three separate tasks: (1) to demonstrate that the FDT Cell would indeed be subcritical under normal conditions and credible upset conditions, (2) to develop a benchmark that could be related to the FDT Cell, and (3) to show that the benchmark case was representative of the FDT Cell problem.

4.1 FDT CELL MODEL DISCUSSION

Several difficulties were encountered while developing the FDT Cell model in KENO V.a. The manufacturing drawings were made available, thus allowing the FDTs and FFTs to be modeled accurately. The problems involved trying to determine the exact composition and quantity of the material in each tank. Different documentation presented slightly different fuel salt compositions and fissile isotope concentrations that could produce significant differences in the resulting k_{eff} values. The final salt composition modeled in the FDT Cell consists of a compromise between several sources. The final FDT and FFT salt parameters used in the FDT Cell model are listed in Tables 1 and 2.

Using the parameters listed in Tables 1 and 2, the FDT Cell was modeled under normal and credible upset conditions. Four different cross-section sets were used to calculate the FDT Cell, resulting in a 13% spread in the system k_{eff}. The cross-section set producing the highest k_{eff} for the normal FDT Cell case was then used to calculate the nominal credible upset condition case. A k_{eff} of 0.8604 and a k_{eff} of 0.9067 were calculated for the normal FDT Cell configuration and for the nominal credible upset FDT Cell configuration, respectively. Both of these results have acceptable subcriticality margins.

Since the precise amount and composition of the material in the FDTs and FFT is in question, sensitivity studies were done on the FDT Cell. Separate $\pm 5\%$ changes in the FDT fissile isotope concentration and salt content resulted in a maximum change of 4.23% in the system k_{eff}. This maximum change was the result of a 5% increase in salt content, thus decreasing the actual fissile fuel density. The system is sufficiently undermoderated, so the additional salt has a larger effect on the reactivity of the system than the addition of the same percentage of fissile fuel.

Several additional parameters related to the FDT Cell were also investigated. The removal of the thimbles and bayonet tubes, which seem to act as a neutron poison, produced a 3.75% increase in k_{eff}. A 10% shift in the salt content from FDT-2 to FDT-1 increased k_{eff} 3.42%. Finally, FDT-1 was analyzed as a single bare tank and a single reflected tank producing

k_{eff} values of 0.8547 and 0.8754, respectively. These values indicate that up to half of the increased reactivity in the nominal credible upset condition case is due solely to the increased reflection around the most reactive FDT. The other half of the 5% reactivity increase is due to the increased neutron interaction between the tanks. This indicates there is little interaction between separate tanks, with the most reactive tank alone having a k_{eff} of over 96% of the nominal credible upset case k_{eff}.

A simplified 1-D FDT model was then constructed in XSDRN consisting of concentric spheres, with the entire salt content of FDT-1 and -2 as the innermost region of the spheres. The variations in the results matched those of the FDT Cell results for each cross-section set. This indicates the difference in results is caused by the cross-section libraries and not the way KENO V.a is using them.

The FDT Cell normal and credible upset condition cases have been shown to remain significantly subcritical for the range of parameters examined. The question remains—does the examined range of parameters encompass the most probable range of the major parameters? Attachment 1 of ref. 15 (NSR0039WM00013A) is a table containing the maximum and minimum values of the material which make up the FDT and FFT salt. Tables 14 and 15 compare the nominal, maximum, and minimum FDT and FFT salt material quantities for the study done in this report with the maximum and minimum FDT material quantities listed in ref. 15.

All material quantities for the FDT salt listed in ref. 15 are bracketed by the maximum and minimum quantities of this study with the exception of the plutonium, as shown in Table 14. The maximum quantity of plutonium in the NSR is about 5.5 g larger than the maximum quantity used in this study. This value is insignificant for two reasons: (1) the small quantity of plutonium will not have a significant effect on this large a system with the level of subcriticality shown, and (2) the reactivity effect of this small quantity of plutonium is more than compensated for by over 1 kg of uranium in excess of the NSR's maximum quantity. Additional characteristics of this study which increased the calculated k_{eff} include: the addition of more salt which acts as a moderator, shifting more salt from FDT-2 into FDT-1, and the lack of any salt impurities which act as neutron poisons.

Table 14. FDT fuel salt parameter comparison between the study done in this report and NSR0039WM00013A

Parameter	This report minimum	NSR minimum	This report nominal	NSR maximum	This report maximum
Total salt mass, kg	4473.3	4650.5	4708.8	4845.7	4944.2
Salt mass in FD-1, kg	2384.3	2478.7	2509.8	2582.7	2760.8
Salt mass in FD-2, kg	1948.0	2171.8	2199.0	2263.0	2308.9
Salt density, g/cm^3	2.35	2.48	2.47	2.48	2.59
U isotopic comp, kg					
^{233}U	28.955	30.479	30.479	31.100	32.003
^{234}U	2.580	2.716	2.716	2.771	2.852
^{235}U	0.883	0.929	0.929	0.948	0.975
^{236}U	0.036	0.038	0.038	0.039	0.040
^{238}U	2.050	2.158	2.158	2.202	2.266
Total U mass, kg	34.504	36.32	36.320	37.06	38.136
Pu isotopic comp, g					
^{239}Pu	577.79	608.4	608.20	643.5	638.61
^{240}Pu	61.03	64.2	64.24	68.0	67.45
^{238,241,242}Pu	2.23	2.4	2.35	2.5	2.47
Total Pu mass, g	641.05	675.0	674.79	714.0	708.53
Fuel salt comp, kg					
LiF	1886.0	1923.9	1985.3	2028.9	2084.5
BeF_2	1601.0	1640.2	1685.3	1717.3	1769.6
ZrF_4	939.8	938.9	989.3	1050.1	1038.8
UF_4	45.7	49.3	48.1	50.1	50.5
PuF_3	0.80	0.8	0.84	0.9	0.88
Salt impurities, ppm					
Cr	--	92	--	98	--
Fe	--	199	--	265	--
Ni	--	--	--	72	--

Table 15. FFT salt parameter comparison between the study done in this report and NSR0039WM00013A

Parameter	NSR minimum	This report nominal	NSR maximum
Flush salt mass, kg	4265.0	4300.6	4274.0
Flush salt density, g/cm^3	2.22	2.47	2.22
Uranium isotopic comp, g			
^{233}U	187.2	190.0	198.7
^{234}U	17.0	20.0	18.3
^{235}U	83.6	90.0	86.6
^{236}U	1.2	0.0	01.2
^{238}U	201.0	190.0	185.2
Total uranium mass, g	490.0	490.0	490.0
Plutonium isotopic comp, g			
^{239}Pu	27.44	13.0	65.37
^{240}Pu	1.41	2.0	3.30
^{241}Pu	0.13	0.0	0.30
^{242}Pu	0.02	0.0	0.03
Total plutonium mass, g	29.0	15.0	69.0
Salt comp, kg			
LiF	2140.2	2226.9	2148.9
BeF_2	2082.2	2073.1	2090.4
ZrF_4	41.8	--	33.8
UF_4	0.6	0.65	0.7
Salt impurities, ppm			
Cr	88	--	93
Fe	146	--	155
Ni	46	--	49

Table 15 contains the comparison of the NSR material quantities in the FFT with those used in this study. The material quantities in the FFT were not modified from the nominal value in this study. Some material differences are noted between the two sets of values, although none would significantly affect the final result of the system. Approximately 0.6% more salt is assumed in this study than the maximum amount listed in ref. 15. The assumed salt composition is also different, having no ZrF_4. The salt is also assumed to be 11% denser and contain no impurities. These variations would have a positive effect on the criticality of the system. The amount of uranium assumed in this study falls between the maximum and minimum quantities listed in ref. 15. The most significant difference is in the amount of plutonium assumed. This study assumed 15 g of plutonium in the FFT, while ref. 15 lists 29 g and 69 g as the minimum and maximum amounts, respectively. These values constitute a significant portion of the fissile material in the system. However, the FFT does not significantly contribute to the criticality of the system, so these differences are not significant.

4.2 REACTOR MODEL DISCUSSION

Similar difficulties were noted with the reactor model that were previously encountered with the FDT Cell model, the worst one being the exact composition of the fuel salt. The fluoride composition and density of the salt were finally taken from ref. 10, assuming an operating temperature of 650°C. The fissile material content (uranium and plutonium) of the reactor was then calculated based on the slug of salt left in the bottom of the reactor and the amount that was added to the fuel salt. Table 7 lists the composition of the fuel salt assumed in the reactor model for the cases analyzed. The reactor model was analyzed using the same cross-section libraries used to analyzed the FDT Cell model. This time the results varied by only 2.27%.

Because several material parameters were not precisely known, sensitivity studies were performed on the reactor system. The same cross-section library used for the FDT sensitivity studies (27GROUPNDF4 library) was used for these studies. Separate $\pm 5\%$ changes were made in the control rod material density, fissile isotope density, graphite density, and fuel salt density. The resulting k_{eff} values changed from a low of 0.9819 (-2.27%) to a high of 1.0191 (1.41%), with the largest change attributed to the change in graphite moderator density. The largest change in reactivity resulted from decreasing the reactor temperature from 650°C to 20°C. Over 6% excess reactivity is needed to bring the reactor to critical at its operating temperature.

The reactor model, although very detailed, was not precise. Other reactor parameters were examined to see if they could be duplicated with the reactor model. An experiment done on the MSRE after the initial ^{233}U fuel loading was done to determine the reactivity worth of the three control rods. An attempt was made to duplicate a portion of that curve using the

reactor model. First, all three rods were inserted as a bank at various positions and analyzed using two different cross-section libraries. The results of this study, given in Tables 10 and 11, show the percentage change in reactivity is relatively insensitive to cross-section libraries.

Using the 27GROUPNDF4 cross-section library, while keeping control rods 2 and 3 at the 51-in. withdrawn position, control rod 1 was inserted at various locations. Table 12 contains the resulting k_{eff} values and calculated percentage changes in reactivity for each rod position. Figure 7 shows excellent agreement between the percentage change in reactivity with respect to rod position for both the initial experiment and the reactor model. This agreement seems to indicate the reactor model is a good representation of the MSRE reactor.

4.3 FDT CELL/REACTOR COMPARISON DISCUSSION

For the reactor model to be an acceptable benchmark for the FDT model, the two systems must have common characteristics in terms of configuration, materials, and neutron energies. From a configuration standpoint, the systems are very similar. Both are large tanks containing a homogeneous fuel salt. The primary difference, however, is that the FDTs contain thimbles, which are net neutron absorbers, and the reactor contains a graphite moderator, control rods, and a specimen array.

The materials in the two systems are almost identical. The fuel salts in the two systems vary only slightly in composition. All vessels are made out of Hastelloy-N surrounded by similar insulation and canning. The primary difference between the reactor system and FDT system is the graphite moderator and control rods in the reactor. The primary effect of the graphite is to lower the average neutron energy in the system.

The difference in the neutronics of the two systems is readily apparent from the energy spectrum of the neutrons inducing fission. Figure 8 contains a graph of the fission-inducing neutron energy spectrum for both the reactor and FDT systems. The average neutron energy is much lower in the reactor than in FDTs primarily due to the graphite moderator. Both systems seem to contain two peaks: an epithermal peak at the 14th energy group and a thermal peak at the 23rd energy group.

In the FDTs the fuel salt is the only moderator. The lack of any further moderation produces an average fission neutron energy group of about 17, with approximately 67% in the epithermal range and 33% in the thermal range. In the reactor, the fuel salt also acts as a moderator, but the majority of moderation is caused by the graphite stringers. This extra moderation produces an average fission neutron energy group of about 21, with approximately 26% in the epithermal range and 74% in the thermal range. Very little fast fission is noted in either system. Both systems are significantly undermoderated, which results in a negative temperature coefficient of reactivity. The presence of two distinct peaks at approximately the

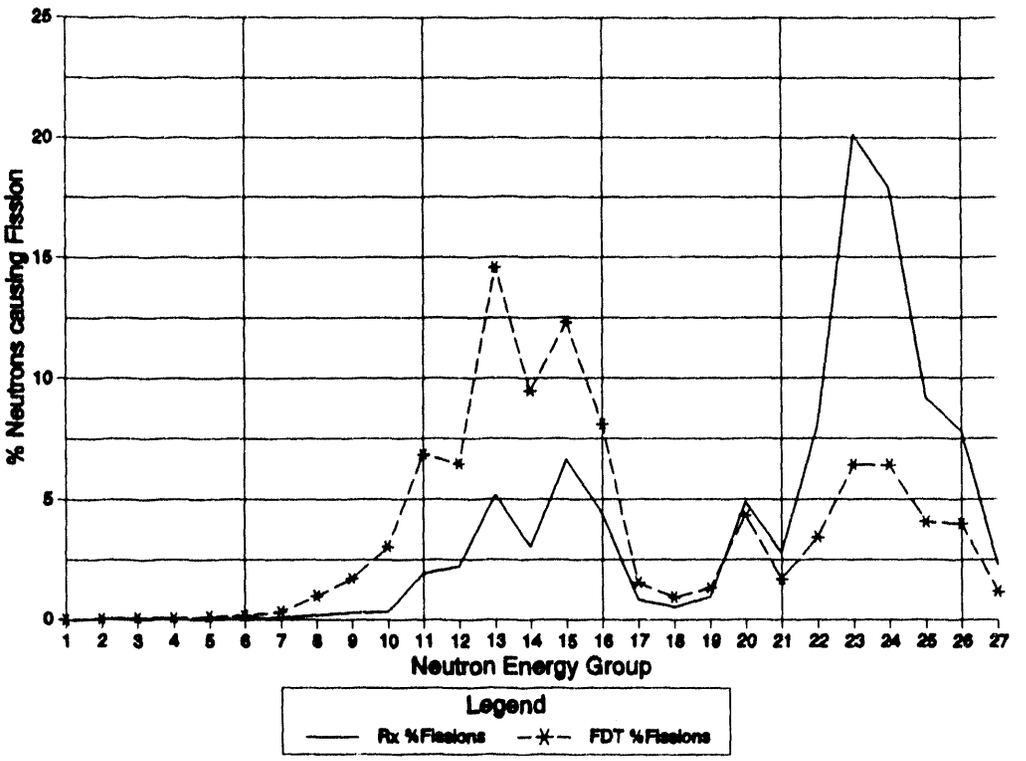

Fig. 8. Percentage of neutrons per energy group that cause fissioning for the reactor and FDT models.

same energy level for the reactor and FDT cell cases is encouraging even if the magnitude of the two peaks is reversed.

The reactor model does indeed have some major differences from the FDT Cell model. However, there are enough similarities to make the reactor model a useful benchmark for the FDT Cell.

4.4 CONCLUSIONS

The FDT Cell was analyzed under normal and credible upset conditions and found to have an acceptable margin of subcriticality under all conditions. The cross-section library and materials were chosen to ensure a conservative result. The 27GROUPNDF4 cross-section library produced the highest k_{eff} for the FDT model and the lowest k_{eff} for the reactor model. The results of the FDT Cell model ran from 0.7514 (0.0015) using Hansen-Roach cross sections to 0.8692 (0.0021) using 27GROUPNDF4 cross sections for a spread of 13%. The 27GROUPNDF4 cross-section library was used for the continuing analysis because it produced

the most conservative results. For the reactor model the Hansen-Roach cross sections produced the highest k_{eff} of 1.0276 (0.0017) and the 44GROUPNDF5 cross-section library produced the lowest k_{eff} of 0.9805 (0.0016) for a spread of 5%. The 27GROUPNDF4 cross-section library, which produced a k_{eff} of 1.0068 (0.0014), was chosen for the additional studies because it was used for the FDT Cell studies and it gave reasonable results. Further conservative biases were introduced in the FDT Cell calculations by using Magnuson concrete, not modeling the thermocouple thimble, level probes, and salt lines, and ignoring fission and corrosion products.

To enhance the confidence level associated with the FDT Cell results, a benchmark having characteristics as close to the FDT Cell as possible was modeled and analyzed. The benchmark results, consisting of the MSRE reactor containing the fuel salt that was eventually stored in the FDT Cell, agree reasonably well with previously documented conditions. Sensitivity studies on both systems were done by varying major parameters $\pm 5\%$. Most of the major parameters are known within about 2%, thus giving an added level of conservatism. As long as the basic assumptions are observed, the FDT Cell is in an acceptably subcritical state.

REFERENCES

1. R. C. Robertson, *MSRE Design and Operations Report, Part I, Description of Reactor Design*, ORNL/TM-728, Union Carbide Corp., Nucl. Div., Oak Ridge Natl. Lab., January 1965.

2. S. E. Beall, P. N. Haubenreich, R. B. Lindauer, J. R. Tallackson, *MSRE Design and Operations Report, Part V, Reactor Safety Analysis Report*, ORNL/TM-732, Union Carbide Corp., Nucl. Div., Oak Ridge Natl. Lab., August 1964.

3. K. J. Notz, *Extended Storage-in-Place of MSRE Fuel Salt and Flush Salt*, ORNL/TM-9756, Union Carbide Corp., Nucl. Div., Oak Ridge Natl. Lab., September 1985.

4. K. J. Notz, *Decommissioning of the Molten Salt Reactor Experiment, A Technical Evaluation*, ORNL-RAP-17, Martin Marietta Energy Systems, Inc., Oak Ridge Natl. Lab., January 1988.

5. L. M. Petrie and N. F. Landers, "KENO V.a: An Improved Monte Carlo Criticality Program with Supergrouping," Sect. F11 of *SCALE: A Modular Code System for Performing Standardized Computer Analyses of Licensing Evaluations*, NUREG/CR-0200 (ORNL/NUREG/CSD-2), Rev. 4, Vols. I, II, and III (draft February 1990). Available from Radiation Shielding Information Center as CCC-545.

6. G. R. Handley, R. C. Robinson, and J. C. Cline, "Effects of Concrete Composition in Nuclear Criticality Calculations," *Trans. Am. Nucl. Soc.* **61**, 182 (1990).

7. Internal Correspondence, R. E. Thoma to R. H. Guymon, "Inventory of Residual Uranium and Plutonium in the MSRE," MSR 71-2, January 7, 1971.

8. R. H. Guymon, *MSRE Procedures for the Period Between Examination and Ultimate Disposal*, ORNL/TM-3253, Union Carbide Corp., Nucl. Div., Oak Ridge Natl. Lab., February 10, 1971.

9. Request for Nuclear Safety Review and Approval, Dated 2/28/90, attachment 10, INTERNAL CORRESPONDENCE dated March 23,1971, To: R. G. Affel, Subject: NSR-577 Criticality Review of the MSRE Drain Tanks Y-DR-58.

10. Stanley Cantor, *Density and Viscosity of Several Molten Fluoride Mixtures*, ORNL/TM-4308, Union Carbide Corp., Nucl. Div., Oak Ridge Natl. Lab., March 1973.

11. J. R. Engel and B. E. Prince, *Zero-Power Experiments with ^{233}U in the MSRE*, ORNL/TM-3963, Union Carbide Corp., Nucl. Div., Oak Ridge Natl. Lab., December 1972.

12. R. E. Thoma, *Chemical Aspects of MSRE Operations*, ORNL-4658, Union Carbide Corp., Nucl. Div., Oak Ridge Natl. Lab., December 1971.

13. G. M. Tolson and A. Taboada, *MSRE Control Elements: Manufacture, Inspection, Drawings, and Specifications*, ORNL-4123, Union Carbide Corp., Nucl. Div., Oak Ridge Natl. Lab., July 1967.

14. B. E. Prince et al., *Zero-Power Physics Experiments on the Molten-Salt Reactor Experiment*, ORNL-4233, Union Carbide Corp., Nucl. Div., Oak Ridge Natl. Lab., February 1968.

15. Mark Ford, Draft Request of Nuclear Safety Review and Approval, NSR0039WM00013A, "MSRE Fuel and Flush Salt Storage," October 28, 1993.

APPENDIX A

DRAWING LISTS FOR THE MSRE REACTOR AND FUEL DRAIN TANK CELLS

MSRE REACTOR DRAWINGS

E-BB-B-40400	REACTOR ASSEMBLY PLAN
E-BB-B-40401	REACTOR ASSEMBLY SECTION SHEET No. 1
E-BB-B-40402	REACTOR VESSEL SHELL, FLOW DISTRIBUTOR AND BOTTOM HEAD ASSEMBLY
D-BB-B-40403	REACTOR VESSEL BOTTOM HEAD ASSEMBLY
D-BB-B-40404	REACTOR VESSEL HEAD - TOP
D-BB-B-40405	REACTOR VESSEL HEAD - BOTTOM DETAILS
D-BB-B-40406	REACTOR VESSEL SHELL
D-BB-B-40407	REACTOR VESSEL FLOW DISTRIBUTOR ASSEMBLY
D-BB-B-40408	REACTOR VESSEL FLOW DISTRIBUTOR DETAILS - SHEET No. 1
D-BB-B-40409	REACTOR VESSEL FLOW DISTRIBUTOR DETAILS - SHEET No. 2
D-BB-B-40410	REACTOR CORE SHELL ASSEMBLY
D-BB-B-40411	REACTOR CORE SHELL DETAILS - SHEET No. 1
D-BB-B-40412	REACTOR CORE SHELL DETAILS - SHEET No. 2
D-BB-B-40413	REACTOR CORE GRID ASSEMBLY
D-BB-B-40414	REACTOR CORE GRID DETAILS - SHEET 1
D-BB-B-40415	REACTOR CORE GRID DETAILS - SHEET No. 2
D-BB-B-40416	REACTOR CORE BLOCK ASSEMBLY PLAN
D-BB-B-40417	REACTOR CORE BLOCK DETAILS - SHEET No. 1
D-BB-B-40418	REACTOR CORE BLOCK DETAILS - SHEET No. 2
D-BB-B-40419	REACTOR CORE BLOCK DETAILS - SHEET No. 3
D-BB-B-40420	REACTOR CORE LATTICE BLOCK ASSEMBLY
D-BB-B-40421	REACTOR CORE LATTICE BLOCK DETAILS - SHEET No. 1
D-BB-B-40422	REACTOR CORE LATTICE BLOCK DETAILS - SHEET No. 2

D-BB-B-40424	REACTOR CORE BLOCK CENTERING BRIDGE
D-BB-B-40427	REACTOR CORE FLOW RESTRICTOR RING - ASSY AND DETAILS
D-BB-B-40428	REACTOR CORE BLOCK RETAINER RING AND RETAINER HOLDING RING ASSEM'S DETAILS
D-BB-B-40429	REACTOR CORE SHELL DETAILS - SHEET No. 3
D-BB-B-40491	REACTOR CORE BLOCK DETAILS - SHEET No. 4
D-BB-B-40493	REACTOR CORE BLOCK AND GRID ASSEMBLY - SECTION
D-BB-B-40494	REACTOR CORE BLOCK AND CORE SHELL ASSEMBLY
D-BB-B-40581	REACTOR CORE BLOCK DETAILS - SHEET No. 5
E-BB-B-40594	REACTOR ASSEMBLY - SECTION SHEET No. 2
E-BB-B-40598	REACTOR CONTROL ROD THIMBLE ASSEMBLY AND DETAILS
E-BB-B-40599	REACTOR ACCESS PLUG SHELL ASSEMBLY AND DETAILS
E-GG-A-40700	FUEL AND COOLANT SALT SYSTEM PIPING REACTOR CELL PLAN
E-GG-B-40701	REACTOR CELL ELEV. LOOKING EAST
E-KK-D-40722	REACTOR CELL REACTOR THERMAL SHIELD WALL SUPPORT
E-KK-D-40723	REACTOR CELL REACTOR THERMAL SHIELD BASE
E-BB-D-40724	REACTOR THERMAL SHIELD ASSEMBLY AND SECTIONS
E-BB-D-40725	REACTOR THERMAL SHIELD SECTIONS AND DETAILS
E-BB-D-40726	REACTOR THERMAL SHIELD PLUGS AND DETAILS
E-BB-D-40727	REACTOR THERMAL SHIELD REMOVAL COVER
E-BB-D-40728	REACTOR THERMAL SHIELD MISCELLANEOUS DETAILS
E-BB-D-40729	REACTOR THERMAL SHIELD ELEVATION
E-BB-D-40730	REACTOR THERMAL SHIELD PLAN
D-AA-A-40880	FUEL SYSTEM PROCESS FLOW SHEET

E-MM-B-56223	REACTOR HEATING ASSEMBLY
E-MM-B-56226	REACTOR RESISTANCE HEATER ASSY - UNIT I
E-MM-B-56227	REACTOR RESISTANCE HEATER ASSY - UNIT II
E-MM-B-56228	REACTOR RESISTANCE HEATER DETAILS
E-MM-B-56229	REACTOR RESISTANCE HTR AND HEATING ASSY - DETAILS
E-BB-B-56346	CONTROL ROD BOTTOM THIMBLE ASSEMBLY AND DETAILS
E-BB-B-56347	REACTOR CONTROL RODS ASSEMBLY AND DETAILS
E-BB-B-56348	HOLD DOWN PLATE FOR REMOVABLE GRAPHITE CORE BLOCKS ASSEMBLY AND DETAILS

MSRE FUEL DRAIN TANK CELL DRAWINGS

D-FF-A-40456	MSRE FDT COOLING SYSTEM ASSEMBLY AND DETAILS
D-FF-A-40457	MSRE FUEL DRAIN TANK ASSEMBLY AND DETAILS FDT No. 1
D-FF-A-40458	MSRE FUEL DRAIN TANK UPPER HEAD ASSEMBLY AND DETAILS FDT No. 1
D-FF-A-40459	MSRE FUEL DRAIN TANK DETAILS
D-FF-A-40460	MSRE FUEL DRAIN TANK SHELL AND LOWER HEAD ASSY AND DETAILS
D-FF-A-40462	FUEL SALT SYSTEM FLUSH TANK ASSEMBLY AND DETAILS
D-FF-A-40463	MSRE FDT COOLING SYSTEM STEAM DOME UPPER HEAD ASSEMBLY AND DETAILS
D-FF-A-40464	MSRE FDT COOLING SYSTEM STEAM DOME UPPER HEAD DETAILS
D-FF-A-40465	MSRE FDT COOLING SYSTEM STEAM DOME LOWER HEAD ASSY AND DETAILS
E-GG-D-40709	PIPING IN REACTOR FUEL FLUSH AND DRAIN TANK CELL - ELEV. "A - A"
D-AA-A-40881	MOLTEN SALT REACTOR EXPERIMENT COOLANT SYSTEM PROCESS FLOW SHEET
D-AA-A-40882	FUEL DRAIN TANK SYSTEM PROCESS FLOW SHEET MSRE
E-FF-D-41500	MSRE FUEL DRAIN TANK SUPPORTING STRUCTURE AND WEIGH ASSEMBLY
E-FF-D-41501	MSRE FUEL DRAIN TANK SUPPORT RING ASSEMBY
E-FF-D-41502	MSRE FUEL DRAIN TANK SUPPORT PEDESTAL AND WEIGH CELL MOUNT
E-FF-D-41503	MSRE COOLANT SALT DRAIN TANK SUPPORT ASSEMBLY
E-FF-D-41504	MSRE COOLANT SALT DRAIN TANK SUPPORT DETAILS

E-GG-D-41512	MSRE PIPING IN REACTOR FUEL FLUSH AND DRAIN TANK CELL - PLAN - SHEET 2
E-MM-B-51610	MSRE FUEL DRAIN AND FLUSH TANKS 8 UNIT HEATER ASSEMBLY SHEET - 1
E-MM-B-51611	MSRE FUEL DRAIN AND FLUSH TANKS 8 UNIT HEATER ASSEMBLY SHEET - 2
E-MM-B-51612	MSRE FUEL DRAIN AND FLUSH TANKS 8 UNIT HEATER DETAILS
E-MM-B-51613	MSRE FUEL DRAIN AND FLUSH TANKS 4 UNIT HEATER ASSY SHEET - 1
E-MM-B-51614	MSRE FUEL DRAIN AND FLUSH TANKS 4 UNIT HEATER ASSY SHEET - 2
E-MM-B-51615	MSRE FUEL DRAIN AND FLUSH TANKS 4 UNIT HEATER DETAILS
B-MM-B-51616	FUEL DRAIN AND FLUSH TANKS CERAMIC HEATER UNIT MSRE
E-MM-B-51652	HEATER AND INSULATION ASSEMBLY FUEL DRAIN AND FLUSH TANKS MSRE
E-MM-B-51684	MSRE FUEL DRAIN TANK NOS. 1 AND 2 AND FUEL FLUSH TANK HEATER AND INSULATION ASSEMBLY - SHEET NO. 1
E-NN-B-51685	MSRE DRAIN AND FLUSH TANKS - TYP ELEVATION THEATER AND INSULATION ASSEMBLY - SHEET NO. 2
E-MM-B-51686	MSRE FUEL DRAIN TANK NOS. 1 AND 2 AND FUEL FLUSH TANK HEATER AND INSULATION CAN ASSEMBLIES
E-MM-B-51687	MSRE FUEL DRAIN TANK NO. 1 HEATER AND INSULATION CAN DETAILS
E-MM-B-51688	MSRE FUEL DRAIN TANK NO. 1 HEATER AND INSULATION CAN DETAILS
E-MM-B-51689	MSRE FUEL DRAIN TANK NO. 1 HEATER AND INSULATION COVER ASSEMBLY
E-MM-B-51690	MSRE FUEL DRAIN TANK NO. 1 HEATER AND INSULATION COVER DETAILS

E-MM-B-51691	MSRE FUEL DRAIN TANK NO. 1 HEATER AND INSULATION COVER - DETAILS
E-MM-B-51692	MSRE FUEL DRAIN TANK NO. 2 HEATER AND INSULATION CAN DETAILS
E-MM-B-51693	MSRE FUEL SALT FLUSH TANK HEATER AND INSULATION CAN DETAILS
E-MM-B-51694	MSRE FUEL DRAIN TANK NO. 2 HEATER AND INSULATION COVER ASSEMBLY
E-MM-B-51695	MSRE FUEL DRAIN TANK NO. 2 HEATER AND INSULATION COVER DETAILS
E-MM-B-51696	MSRE FUEL SALT FLUSH TANK HEATER AND INSULATION COVER ASSEMBLY
E-MM-B-51697	MSRE FUEL SALT FLUSH TANK HEATER AND INSULATION COVER - DETAILS

INTERNAL DISTRIBUTION

1. J. F. Alexander
2. J. E. Bigelow
3. S. M. Bowman
4. B. L. Broadhead
5. R. L. Chadwick
6. T. J. Cofer
7. W. K. Crowley
8. E. C. Crume, Jr.
9. H. R. Dyer
10-14. M. K. Ford
15. H. R. Gaddis
16. N. M. Greene
17-21. D. F. Hollenbach
22-26. C. M. Hopper
27. W. C. Jordan
28. N. F. Landers
29. G. A. Mays
30. L. E. McNeese
31. D. E. Mueller
32. L. F. Norris
33. C. V. Parks
34. L. M. Petrie
35. J.-P. Renier
36-37. C. H. Shappert
38. G. R. Smolen
39. S. G. Snow
40. R. V. Stachowiak
41. J. C. Turner
42. R. M. Westfall
43. G. E. Whitesides
44. R. Q. Wright
45-47. Laboratory Records Department
48. Laboratory Records, ORNL-RC
49. ORNL Y-12 Research Library Document Reference Section
50. Central Research Library
51. ORNL Patent Office

EXTERNAL DISTRIBUTION

52. Office of the Deputy Assistant Manager for Energy Research and Development, Department of Energy Oak Ridge Operations (DOE-ORO), P.O. Box 2008, Oak Ridge, TN 37831-6269
53-54. Office of Scientific and Technical Information, U.S. Department of Energy, P.O. Box 62, Oak Ridge, TN 37831

DATE FILMED

4/5/94

END